

A hybrid heterojunction based on fullerenes and surfactant-free, self-assembled, closely packed silicon nanocrystals

This article has been downloaded from IOPscience. Please scroll down to see the full text article.

2010 J. Phys. D: Appl. Phys. 43 415402

(<http://iopscience.iop.org/0022-3727/43/41/415402>)

View [the table of contents for this issue](#), or go to the [journal homepage](#) for more

Download details:

IP Address: 193.61.144.108

The article was downloaded on 30/09/2010 at 11:11

Please note that [terms and conditions apply](#).

A hybrid heterojunction based on fullerenes and surfactant-free, self-assembled, closely packed silicon nanocrystals

V Švrček¹, D Mariotti², Y Shibata¹ and M Kondo¹

¹ Research Center for Photovoltaics, National Institute of Advanced Industrial Science and Technology (AIST), Central 2, Umezono 1-1-1, Tsukuba, 305-8568, Japan

² Nanotechnology & Advanced Materials Research Institute (NAMRI), University of Ulster, Shore Road, Newtownabbey, Antrim, BT37 0QB, UK

E-mail: vladimir.svrcek@aist.go.jp

Received 24 February 2010, in final form 12 August 2010

Published 29 September 2010

Online at stacks.iop.org/JPhysD/43/415402

Abstract

We demonstrate that nanosecond-pulsed laser chemistry in water leads to closely packed and stable luminescent assemblies of silicon nanocrystals (SiNCs) that can be electronically coupled with fullerenes (C₆₀) without any additional surfactant or catalyst. We show that the fragmentation time in water determines the photoluminescence (PL) intensity (>40%) and redshifts the PL maxima (45 nm) of the SiNCs. Heterojunction solar cells made out of these laser-produced self-assemblies of SiNCs and C₆₀ show photovoltaic action with increased quantum efficiency in the region where the absorption of SiNCs appears.

(Some figures in this article are in colour only in the electronic version)

1. Introduction

Silicon nanocrystals (SiNCs), also referred to as silicon quantum dots, exhibit unique properties that make them very attractive for their use in a wide range of different applications [1, 2]. Optoelectronic properties of SiNCs, for instance, are substantially different from those observed for bulk silicon and can be advantageous for photovoltaic (PV) technologies [3–7]. Fabrication of SiNCs with different crystal sizes (<10 nm) allows controlling the degree of quantum confinement [3] which in turn determines the energy band gap and provides the opportunity for optimizing the SiNCs' absorption spectrum to that of the solar radiation. Moreover, it is believed that the energy conversion efficiency can be drastically improved through SiNC-specific processes such as the generation of multiple charges by single photons (i.e. multiple exciton generation) [8–10]. In addition to the possibility of exploiting new physics for advanced SiNC-based devices, silicon has an advantage over other materials thanks to the existing and established Si-based industrial processes. As a consequence, the transition from traditional silicon technologies to devices

based on SiNCs may represent an affordable step that could ease the deployment of PV and optoelectronic devices with new attractive properties [4].

One of the challenges faced in the development of reliable SiNC-related processes is represented by the difficulties that may be encountered during their manipulation. This is because SiNCs are highly reactive when exposed to oxygen and SiNCs' properties are strongly affected by their surface characteristics. Therefore, SiNCs dispersed in solutions may offer a viable option to overcome these difficulties. The use of SiNC colloidal dispersions may open new possibilities and offer a simple route to tailor the SiNCs' properties [11–13]. For instance SiNC-based inks coupled with low-cost screen printing technologies would allow one to design large scale fabrication processes to deliver suitable large-area architectures for solar cells [14]. The success of these low-cost and screen-printed (or spin coated, etc) architectures also relies on the ability of producing layers with a large number of closely packed SiNCs. Closely packed SiNCs are necessary to enhance carrier transport through percolation trajectories. In

fact, in these architectures, charged carriers are delivered to or from the electrodes through percolated networks [15].

In order to overcome some of these challenges, we have developed a fabrication approach based on nanosecond-pulsed laser fragmentation of electrochemically etched silicon in water [16]. Laser-induced fragmentation has a few advantages compared with other fragmentation techniques in liquid media such as approaches based on ultrasounds [17]. The most important difference is that the laser-induced fragmentation, in addition to efficient separation of particles, offers the opportunity of simultaneous and unique surface chemistry. Thus the surface characteristics of the particles just separated can be modified by laser-induced chemical reactions with no risk of contamination and undesired surface degradation. Particularly, laser processing in water has been demonstrated to be a highly flexible process with the possibility of tuning the material characteristics by varying the processing parameters [18]; for instance, laser processing in water increases the growth rate compared with chemical precipitation [19, 20]. Furthermore, during laser fragmentation, thermal convection and liquid motion can be controlled by adjusting the laser pulse width [18] which also allows the generation of ultrasounds [21]. Finally, the unique chemistry offered by nanosecond laser fragmentation of SiNC micrograins in water allowed the subsequent self-assembly of conductive luminescent SiNC-based networks [16]. The self-assembled networks contain SiNCs that are sufficiently close to each other to permit charge transport over long-range trajectories ($>500 \mu\text{m}$) [16]. Moreover, this laser-based process has the capability of tailoring the SiNCs' surface with a thin oxide layer and exceptional interface passivation [22].

On the other hand, fullerenes (C_{60}) are unique carbon-based nanostructures that have already proven great potential for uses in future nanotechnological and particularly PV applications [23]. C_{60} can accept electrons and are molecules with very good electron transport properties; therefore fullerenes are very attractive for novel nanodevices as they can form junctions with organic or inorganic materials [23]. One can expect that the combination of C_{60} monolayers with closely packed and surfactant-free SiNCs modified by unique laser chemistry in liquid may provide the basis for original physical and chemical properties [24].

In this paper we will demonstrate that SiNCs aggregated in micrometre-sized grains produced by electrochemical etching can be effectively fragmented by a nanosecond-pulsed laser in water. The laser fragmentation process in water can also be used to tune surface characteristics, the photoluminescence (PL) intensity and the PL maxima of the SiNCs. The absorbance properties of laser-processed SiNCs in water (and in ethanol for comparison) have also been measured. Moreover, we show that these surfactant-free SiNCs, when deposited on a substrate, can self-assemble in long-range networks that preserve their stability after subsequent deposition of a C_{60} film coating. The SiNCs and fullerenes are electronically coupled and the formation of a heterojunction is illustrated. The PV action of the heterojunction formed by C_{60} structures and surfactant-free, self-assembled, closely packed SiNCs is revealed.

The electronic coupling between SiNCs and C_{60} structures represents an important step towards the potential future utilization of PV nanoarchitectures that exploit the advantages of both SiNCs and fullerenes, i.e. the possibility of band gap engineering and multiexciton generation together with efficient and rapid exciton dissociation.

2. Experimental details

Similarly to our previous work [16], the powder containing single SiNCs and SiNCs aggregated in micrometre-sized grains (hereafter SiNC micrograins) were produced by electrochemical etching of a silicon wafer (p-type boron doped, $\langle 100 \rangle$, $0.1 \Omega \text{ cm}$, thickness 0.525 mm) and subsequent mechanical pulverization [11, 25]. Then, 2.5 mg of the powder was dissolved in 10 ml of pure water before being processed by the laser fragmentation technique. Since the electrochemically etched powder (SiNCs micrograins) is hydrophobic and fragmentation by nanosecond-pulsed laser requires a homogeneous dispersion of the powder in the liquid media [26], a small amount of ethanol (10 drops) is used to wet the SiNCs micrograins surface in order to achieve a homogeneous colloidal dispersion in water. The fragmentation was conducted by irradiating the solution with a pulsed laser (Kr:F, 245 nm , 20 Hz , $130 \text{ mJ pulse}^{-1}$) at room temperature for different time durations. The laser beam was focused onto a 3 mm diameter spot on the liquid surface by a lens with a focal length of 250 mm . During the irradiation, the glass container was closed and rotated. For comparison, we have also repeated the same process where in place of water we have used ethanol during the fragmentation process.

The experimental solar cells were fabricated as follows. After fragmentation, one droplet of the fragmented SiNCs colloidal dispersion was deposited and allowed to dry on an ITO/PEDOT-coated glass substrate ($\sim 150/150 \text{ nm}$ ITO/PEDOT thickness) within a nitrogen-filled glove box. After water/ethanol evaporation, a 90 nm thick fullerene film was deposited. Finally, 100 nm aluminium electrodes were deposited through a shadow mask. The active area of the device was 4 mm^2 .

Scanning electron microscope (SEM) images were captured with a Hitachi microscope at 20 kV acceleration voltage. External quantum efficiency (EQE) of the full device based on the heterojunction formed by C_{60} structures with the SiNCs was then measured under illumination with monochromatic light from a Xe lamp. In all cases the irradiation intensities were calibrated by a standard a-Si solar cell. An excitation at 400 nm was used to confirm the SiNCs' luminescence properties.

3. Experimental results and discussion

Since the SiNCs micrograins have a significant absorption cross-section in the spectral region from 250 to 500 nm , an optical excitation and fragmentation of the dispersed SiNCs can be effectively achieved in liquid media [26]. The colloidal dispersion, initially turbid, becomes almost transparent after fragmentation, indicating that efficient fragmentation of the

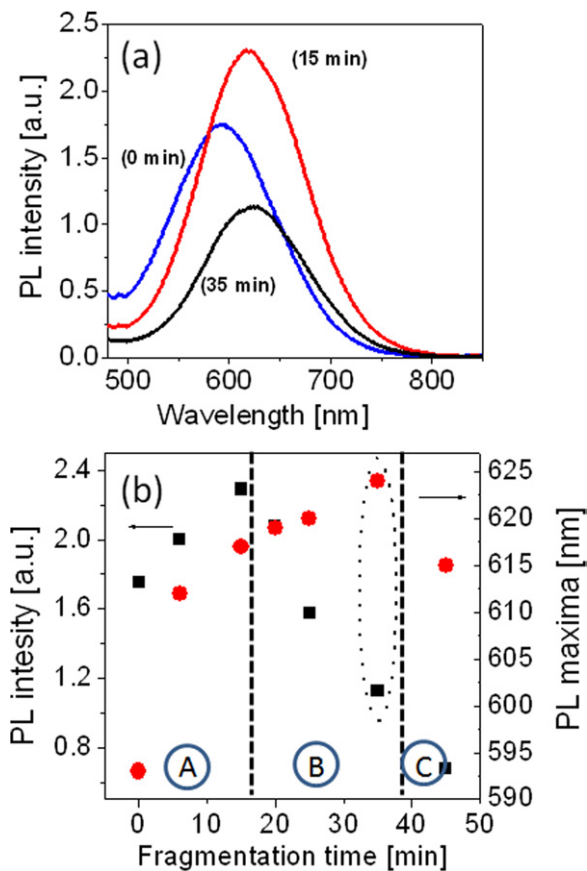


Figure 1. (a) PL spectra of SiNCs after nanosecond laser fragmentation in water at different duration times. The colloidal solutions are excited at 400 nm wavelength. (b) Summary of the PL intensity (black squares) and PL maxima position (red circles) as a function of fragmentation time.

SiNC micrograins has been achieved [16]. Transparency of the colloidal dispersion is reached after prolonged laser fragmentation (>35 min). The presence and quality of SiNCs with quantum confined characteristics (<10 nm diameter) were assessed through visible PL. Figure 1(a) shows the typical PL spectra of SiNCs before ($t = 0$ min, blue line) and after the fragmentation process in water for $t = 15$ min and $t = 35$ min. Since the colloidal dispersions of non-fragmented SiNCs micrograins contain some amount of single SiNCs [11, 16], room temperature PL can be observed in all cases. The width of the broad PL peak is related to the nanocrystals' size distribution and surface states [3]. After the application of the fragmentation process, changes in PL intensity and position of the PL spectra maxima are recorded. Figure 1(b) summarizes the PL intensity maxima (full black squares) and position of the PL maxima (full red circles) as a function of the fragmentation time t . It is observed that during the fragmentation time up to $t = 15$ min, the PL intensity increases and then as the fragmentation continues the intensity is reduced by more than 40%. Interestingly, with increasing fragmentation time, the PL maximum redshifts by about 30 nm (at $t \approx 35$ min).

The absorbance of the colloidal dispersion at different processing times follows a similar trend. Figure 2 shows the absorbance of SiNCs fragmented in water for different times.

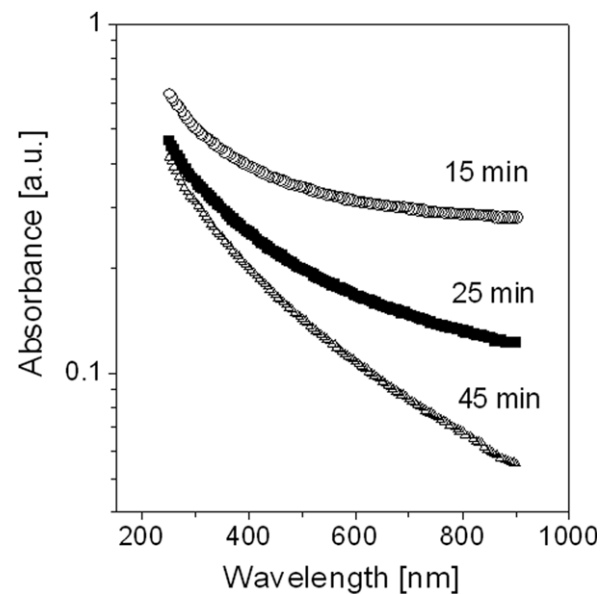


Figure 2. Absorbance of SiNCs fragmented in water for different duration times.

Representative absorption spectra for 15, 25 and 45 min of laser fragmentation are shown. Differences in the slopes of the three absorbance spectra can be easily seen (figure 2). The size distributions of the SiNCs show rather broad band edges and do not allow a precise evaluation of the Tauc gap [27] as it would be necessary to confirm the relatively small gap differences detected by PL measurements. However, a qualitative analysis can corroborate the observations deduced by PL measurements. From figure 2, it is clear that at shorter fragmentation times the gradient of the curve is smaller which indicates a reduced energy band gap. As the fragmentation continues (~ 45 min), the increased slope gradient indicates an opening of the band gap.

Here, it may be useful to recall that within the multiple processes that induce the fragmentation, photothermal heating and Coulomb explosion play an important role [28]. These are followed by the formation of shock waves in the colloidal dispersion that lead to the detachment of nanocrystals that are weakly attached to the micrograins [3, 11, 26]. During this process, first the smallest weakly attached SiNCs are defragmented which leads to increasing PL intensity as more single SiNCs are dispersed in the solution (black squares, up to 15 min). As the fragmentation continues, larger particles are also separated from the larger micrograins and the higher concentration of larger SiNCs in the dispersion leads to the red-shift of the PL maximum. On the other hand it is well documented in the literature that laser-induced chemical processes in water can modify the surface of dispersed particles [19, 20]. Three different processing time frames can be identified in the fragmentation process (A, B and C; see figure 1(b)), which are characterized by the progression of reactions at the surface/near-surface of the SiNCs. FTIR transmission spectra can be used to clarify some of the changes observed at different processing times in the SiNCs' optical properties. Figure 3 shows the transmission spectra for SiNCs at different processing times which are representative of the

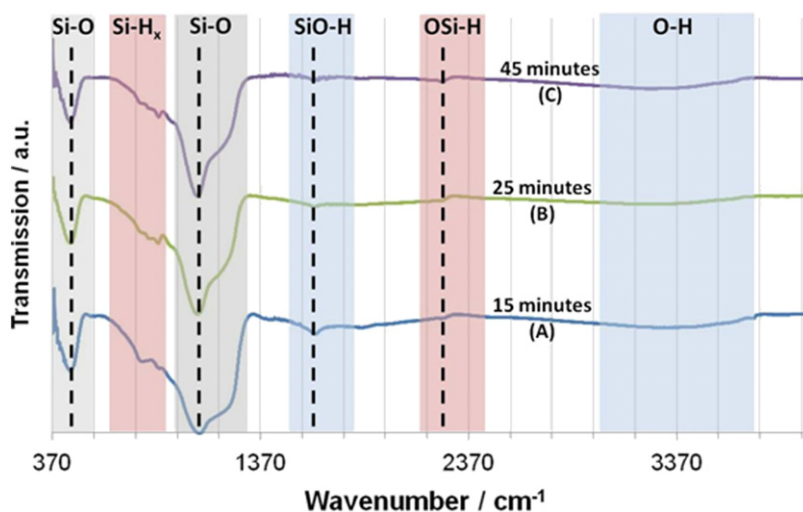


Figure 3. Corresponding FTIR spectra of SiNCs fragmented for different times.

three time frames. The FTIR spectra have been normalized to the lowest transmission peak which resulted as the Si–O peak around 1100 cm^{-1} for all measurements. This is because spectra are not directly comparable as we cannot accurately control the SiNC density used for FTIR measurements.

Initially, in the first 15 min, time frame A (figure 1(b)), the fragmentation process only accelerates reactions that are anyhow occurring at the SiNCs surface when in contact with water. Water promotes partial and incomplete back oxidation [29] as confirmed by Si–O transmission peaks at 450 and 1075 cm^{-1} [30] and the OSi–H peak around 2250 cm^{-1} [31]. The bending vibration of Si–O at 800 cm^{-1} might be too low to be clearly identified and may be overlapping with Si–H bands. Furthermore, during the first 15 min, the higher concentration of OH radicals produced under laser irradiation quickly saturates the possible dangling bonds at the silicon surface forming Si–OH terminations. This can be observed in the 1650 cm^{-1} peak (SiO–H) appearing in the FTIR spectrum; similarly the SiO–H broad band around 3400 cm^{-1} is also observed (figure 3, 15 min). It is believed that region A is due to both detachment of particles from larger grains and chemical passivation. Since the fragmentation and passivation of SiNCs do not change the size distribution significantly the broad PL band remains rather same. The improved surface passivation contributes to the increased PL intensity (in addition to the fragmentation previously mentioned) and the OH terminations might also be responsible for the red-shift as predicted by theoretical calculations [32].

Within the processing time frame labelled B, water radicals that cannot find any longer path for easy surface passivation proceed to react with surface silicon dimers with structure $(\text{SiH})_2$, which are likely the second most energetically favourable reaction sites after unsaturated terminations; Si dimers present long bonds with strained angles and therefore are highly susceptible to reacting with OH. It may be important to note that our SiNC powder before being dispersed in water presents strong FTIR absorption (not shown here) around 626 and 2092 cm^{-1} which are attributed to Si monohydrides with the second peak influenced by Si–Si dimer bonds. OH-induced

cleavage of the Si–Si dimer bonds leads to the formation of one Si–OH and one Si–H termination per dimer. The increased number of Si–H terminations can be related to spectral changes around 770 cm^{-1} . However, no obvious OH transmission change is observed in the FTIR spectra because adjacent OH terminations tend to progress quickly to condensation and accelerated oxidation producing water as a by-product. This process completes the partial oxidation initiated in (A) and a slight increase in the 2250 cm^{-1} peak (corresponding to $\text{O}_3\text{Si-H}$ [31]) may be the proof of this. The reduced shoulder around 1200 cm^{-1} observed after 25 min processing is therefore related to the formation of a higher quality stoichiometric oxide [12] and could be justified by the disappearance of Si dimers at the SiNC surface [33]. However, due to the kinetics of this chain of reactions and in particular due to OH-induced cleavage, the process in (B) does introduce defects in the Si network producing strained bonds [31, 33]. This can be clearly seen in the PL intensity that starts decreasing with 20 min processing time, while the red-shift is slowed down due to a decreased number of reactive sites for the OH radicals and a complete detachment of SiNCs from larger aggregates.

In the last 10 min of processing, time frame C, oxidation proceeds towards the Si core which decreases the photoactive SiNCs' size and consequently blue-shifts the PL maximum. As this oxidation process proceeds quite rapidly, further defects may be introduced contributing to a further decrease in the PL intensity. It is likely that on increasing the processing time further, the PL intensity may stabilize or even increase as the oxide layer is fully completed. However, as the SiNC size is being reduced, other factors may contribute to lower PL intensity (e.g. lower radiative recombination efficiency).

Of course the amount of ethanol used to initially de-wet the SiNCs might affect the process. However, at small concentrations, ethanol does not seem to influence the surface chemistry as indicated by our FTIR spectra and the absence of strong transmission peaks related to C–H or C–O bonds. The best conditions for the synthesis of luminescent SiNCs still need to be found. Also, it has to be considered that

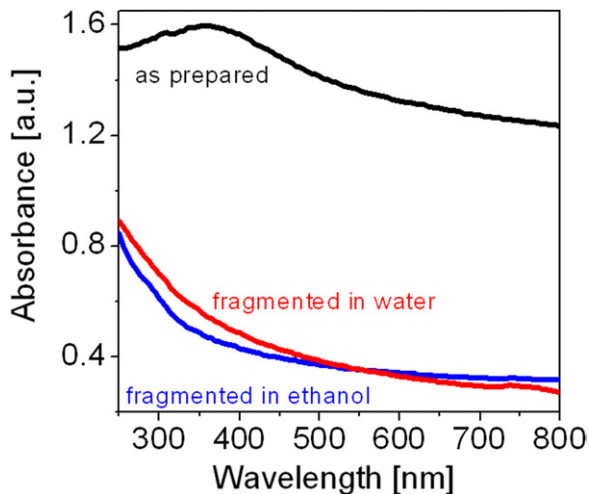


Figure 4. Absorbance of SiNCs as-prepared (black line), fragmented in ethanol (blue line) and water (red line).

the application will largely determine the ideal SiNC surface characteristics so that the ideal junction to be formed between SiNCs and fullerenes might require a surface treatment of SiNCs that is different if the SiNCs were to be employed in a P3HT–SiNC junction [34]. It is now clear that varying the fragmentation time allows one to tune the PL maxima and therefore the energy band gap. This represents, therefore, a simple method for producing nanostructures with optical characteristics that might present a better match to the solar spectrum [2, 4]. Another useful characteristic is the possibility of reducing the radiative recombination rate which can become beneficial for PV applications through the enhancement of the generated photocurrent.

In the rest of this work we have focused on SiNCs produced after about 35 min laser fragmentation corresponding to particles with an average diameter of about 4 nm [3]. At the selected fragmentation time (35 min) both colloidal dispersions (in water and in ethanol) become nearly transparent in the visible spectral region. Figure 4 shows the absorbance of the colloidal dispersion with the as-prepared (i.e. non-fragmented) SiNCs micrograins (black line), after fragmentation in ethanol (blue line) and in water (red line). The measurements show that after fragmentation (blue and red lines) absorption is higher at shorter wavelengths (<400 nm) due to absorption within the nanocrystals' quantum confined states [35]. The gradual increase in absorption with decreasing wavelength corresponds to transitions across the indirect band gap [12, 36]. It can be seen that both fragmentation in water and that in ethanol lead to rather similar absorption features, which is in agreement with previous reports on colloidal SiNCs [36–38]. We would like to stress that at large band gaps (~ 4 eV), absorption across the direct band gap can occur and it is usually observed for only 1–2 nm diameter SiNCs [37, 38]. In our specific case SiNCs with a diameter of around 2 nm may exist in the initial powder of SiNCs micrograins and the fragmentation process would contribute to increasingly release these ultra small crystals into the colloidal dispersion [11]. In addition, the fragmentation process also induces the formation of an oxide layer in larger SiNCs whose core size may be

consequently reduced. Therefore, absorption around or below 300 nm is produced by both SiNCs which were initially small and SiNCs which have developed an oxide shell reducing the core to diameters in the 1–2 nm range. Overall it is, however, difficult to quantitatively attribute the absorption and PL features to direct or indirect transitions and given the broad peak observed we can only suggest that both processes are involved here [11, 12].

In order to evaluate the feasibility of using SiNCs for PV applications, following the laser-based fragmentation process, the colloidal dispersion is deposited on substrates to allow evaporation of water/ethanol and for further processing. We have previously shown [16] that laser interaction with the SiNCs micrograins in water leads to peculiar physics, which results in the self-assembly of percolating networks when the SiNCs are deposited to dry on a substrate. The self-assembled patterns generally consist of interconnected and conductive structures that exceed several hundred micrometres in length ($>500 \mu\text{m}$). The conductivity of the self-assembled network has been previously verified [16] despite the fact that SiNCs have not been treated with surfactants that favour charge transfer. The self-assembly is likely the result of surface non-uniformity on the SiNC micrograins whereby the fragmentation in water contributes to surfactant-free SiNCs. When the SiNCs de-wet, enhanced dipole–dipole interactions induce long-range self-assembly of connected networks. It has to be emphasized that the self-assembly process is specific to this fragmentation process in water and that for instance the same procedure in ethanol does not lead to self-assembly (figure 5(a) in water and figures 5(b) and (c) in ethanol). Fragmentation in ethanol tends to form well-separated large spherical aggregates with an average diameter size of 300 nm (figures 5(b) and (c)). This is most likely due to a low zeta potential that favours a spherical arrangement of the SiNCs [22]. Furthermore the respective arrangements, long-range networks or spherical aggregates, are independent of the substrate material as the same observations are recorded for different materials [16]; here we show images of the colloidal dispersion fragmented in ethanol and deposited on indium tin oxide (ITO) on glass and on glass only (figure 5(b)); in these images a fullerene coating is also present).

The formation of a heterojunction with the SiNCs is achieved by depositing a fullerene coating on the dried SiNCs' colloidal dispersion. The inset of figure 6(a) shows the structure of the measured device. SiNC networks produced in this way do not possess an organic surfactant allowing the direct formation of the junctions possibly through covalent bonds (e.g. Si–C) by simple C_{60} deposition [28]. As mentioned previously, a 35 min fragmentation time was also selected because with these settings the largest red-shift in the PL maxima was observed together with a relatively low PL intensity. The corresponding EQE of the two sample devices is reported in figure 6(a). Due to C_{60} absorption, the EQE of both samples shows an increased signal also above 500 nm. A clear higher EQE can be noticed for the SiNCs fragmented in water (red line) which is believed to be the consequence of the percolation trajectories formed by the self-assembled networks. These long-range conductive networks were not

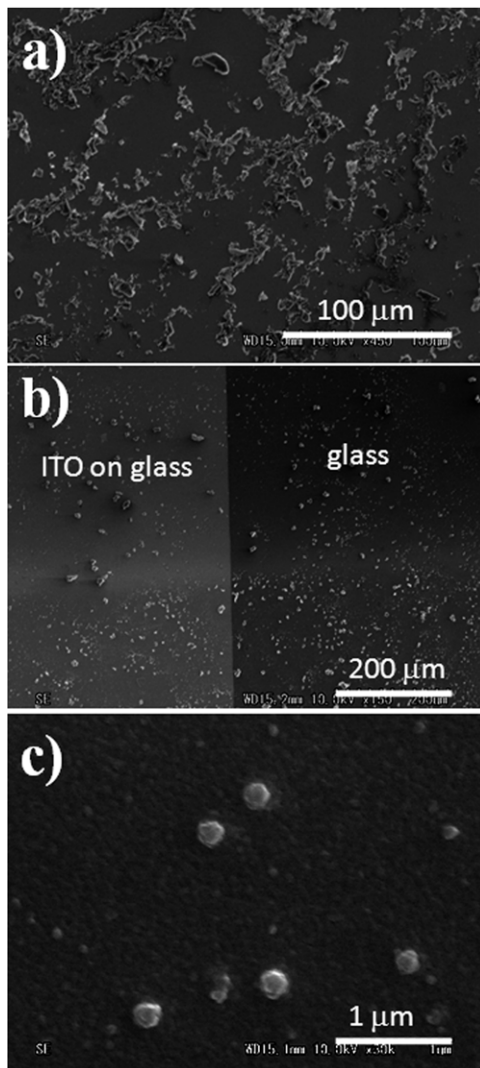


Figure 5. SEM images of SiNCs micrograins fragmented for 35 min in water on PEDOT/ITO on glass (a) and in ethanol (b) on PEDOT/ITO on glass and on PEDOT/glass only. (c) Detailed SEM image of spherical particles formed by samples fragmented in ethanol. All the images were taken after deposition of the C₆₀ layer.

present for SiNCs fragmented in ethanol and contributed to an overall higher photocurrent for the water-fragmented sample. It may be argued that higher EQE for the ‘water’ sample may originate from the differences also observed in the absorption spectrum of figure 4. However, the EQE signal in the longer wavelength region is also enhanced for the water-fragmented sample. This feature is evident in the range 600–700 nm, where the absorption spectrum of the water-fragmented sample is even lower than the ethanol-fragmented one so that could not consistently contribute to a higher EQE.

In figure 6(b) we report the band diagram of the hybrid organic/inorganic device. It is clear from the results that the SiNCs and C₆₀ structures are electronically coupled. The regime of this coupling can be potentially tuned by altering the alignment of SiNCs’ energy states with respect to the fullerenes band edges. With reference to figure 6(b), the absorbed photons striking the SiNCs with energy gap ~ 2 eV create an exciton. The literature reports different values for the

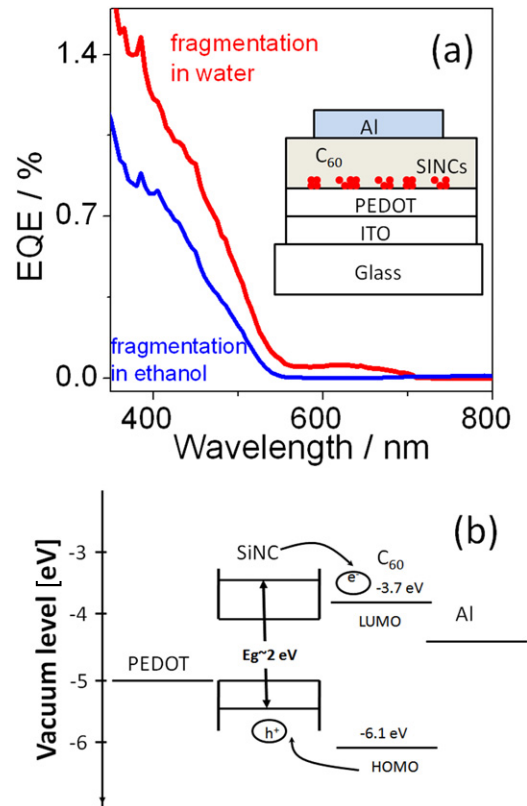


Figure 6. (a) EQE of the device based on micrograins fragmented in ethanol and water after deposition of C₆₀. Inset shows the structure of the measured device. (b) Corresponding band diagram of the device.

position of the fullerene’s HOMO–LUMO values, e.g. LUMO is between -3.7 and -4.5 eV [39, 40]. On the other hand, the conduction band of SiNCs is ~ -3.55 eV [41], which is still higher than any of the C₆₀ LUMO values reported above and allows the formation of a bulk-type heterojunction [42]. Then the differences in electron affinity and ionization potential between the nanocrystals and the fullerenes provide the energy driver for the dissociation of excitons and the consequent photoconductivity. The SiNC–fullerene electronic coupling seems therefore to be justified; however, the architecture of the device requires a careful analysis. In an ideal case, generation of excitons and transport of carriers to the electrodes should rely on optimized processes whereby best utilization of photon energy is achieved and chances of carrier recombination are minimized. However, in our current structure a combination of processes might be occurring which will need to be addressed to clarify the nature of the coupling between SiNCs and fullerenes as well as to optimize the device efficiency. In particular, both SiNCs and C₆₀ might contribute to electron–hole pair generation. Following exciton generation and dissociation possibly at the SiNCs–C₆₀ interface, the electrons and holes take different paths which may include transfer from fullerene to fullerene or from SiNC to SiNC. Eventually, electrons may find a path to the Al electrode and holes can be collected at the PEDOT side. Despite the possibility of these different generation and transport processes, this current device arrangement has shown the potential of coupling surfactant-free SiNCs with fullerenes and producing related

quantum efficiency measurements. The hybrid SiNCs–C₆₀ solar cell shows EQEs over 1.4% at high energies (>400 nm) and a power conversion efficiency of up to ~0.06% in the spectral region 550–700 nm contributing mostly from closely packed SiNCs. Our SEM images showed that in both cases we have no continuous film of SiNCs, rather branched-like structures. It is interesting to note that in the sample with SiNCs fragmented in water, the electrons seem to have fewer chances to recombine, probably due to the self-assembled networks that act as percolating trajectories. The self-assembled network may also affect the energy levels along the connecting paths; however, this second hypothesis remains for the moment a speculation as, at this stage of our work, we do not have any direct evidence to confirm it. In the case of SiNCs fragmented in ethanol, the electrons may remain confined to one or a group of SiNCs before they transfer to the C₆₀ layer, which might increase their recombination chances. The difference between the two quantum efficiency measurements of figure 6(a) is therefore clear evidence of the contribution of SiNCs to the generation of electron–hole pairs and at the same time confirms the electronic coupling with fullerenes.

Future improvements in the direction of this work should aim at the optimization of the solar cell fabrication process and device structure to take advantage of the properties offered by both SiNCs and fullerenes. The factors to be considered in the process design are the SiNCs' PL quantum yield, SiNCs' surface stability, prevention/control of the surface oxidation and stability of the heterojunction to mention a few. It might be useful to mention here that the SiNCs' size can be effectively controlled within the electrochemical etching process which determines the initial size distribution of the aggregated SiNCs. The parameters of the etching process can also be tuned to produce highly absorbing black silicon [43, 44]. The ability of synthesizing SiNCs with different sizes and the possibility of producing self-assembled percolating networks with ease will be beneficial for the complete fabrication of solar cells matched to the solar spectrum. Inclusion of SiNCs with a narrow band gap will eventually result in a PV response that extends from the visible to the near-infrared region. Colloidal dispersions of SiNCs lend themselves quite easily to be used as inks and therefore printing processes may be used for low-cost PV devices based on advanced nanoarchitectures. Furthermore, we believe that the combination of unique low-dimensional electronic properties of SiNCs with fullerenes can have a strong impact on future PV or optoelectronic developments.

4. Conclusion

In conclusion, we have demonstrated that the nanosecond-pulsed laser fragmentation of SiNC micrograins in water can be a useful process for tuning PL intensity and PL peak wavelength. We showed that fragmentation in water can be efficient in controlling the SiNCs' short-range interactions and can determine the subsequent organization of SiNCs on the substrate. The deposition of a fullerene coating has produced a hybrid heterojunction of electronically coupled fullerenes and SiNCs with no need of additional surfactant or catalyst. It was also found that the PV effect is affected by the SiNCs'

arrangement on the substrate and in particular self-assembled SiNCs produced by fragmentation in water have higher EQE. We therefore argue that C₆₀ and SiNCs, with Si and C both abundant in nature, may be important nanostructures for novel devices with unique electronic properties. Our work has shown initial encouraging results for their application in hybrid solar cells.

Acknowledgments

This work was partially supported by a NEDO project and DM JSPS invitation fellowship.

References

- [1] Canham L T 1990 *Appl. Phys. Lett.* **57** 1046
- [2] Koshida N (ed) 2009 *Device Applications of Silicon Nanocrystals and Nanostructures (Nanostructure Science and Technology XII)* 348pp
- [3] Wolkin M V, Jorne J, Fauchet P M, Allan G and Delerue C 1999 *Phys. Rev. Lett.* **82** 197
- [4] Green M 2003 *Third Generation Photovoltaics* (Berlin: Springer)
- [5] Švrček V, Mariotti D, Hailstone R, Fujiwara H and Kondo M 2008 *Proc. MRS 2008 Spring Meeting (San Francisco, CA)* A18.10
- [6] Huang S Y, Arulsamy A D, Xu M, Xu S, Cvelbar U, Mozetic M and Ostrikov K 2009 *Phys. Plasma* **16** 123504
- [7] Cheng Q, Xu S and Ostrikov K 2009 *J. Phys. Chem. C* **113** 14759
- [8] Schaller R D and Klimov V I 2004 *Phys. Rev. Lett.* **92** 186601
- [9] Ellingson R., Beard M C, Johnson J C, Yu P, Micic O I, Nozik A J, Shabaev A and Efros A L 2005 *Nano Lett.* **5** 865
- [10] Beard M C, Knutsen K P, Yu P, Luther J M, Song Q, Metzger W K, Ellingson R J and Nozik A J 2007 *Nano Lett.* **8** 2506
- [11] Švrček V, Slaoui A and Muller J C 2004 *J. Appl. Phys.* **95** 3158
- [12] Sato S and Swihart M T 2006 *Chem. Mater.* **18** 4083
- [13] Jurbergs D, Rogojina E, Mangolini L and Kortshagen U 2006 *Appl. Phys. Lett.* **88** 233116
- [14] Mangolini L and Kortshagen U 2007 *Adv. Mater.* **19** 2513
- [15] Priolo F, Franzo G, Pacifici D and Vinciguerra V 2001 *J. Appl. Phys.* **89** 264
- [16] Švrček V, Mariotti D, Kalia K and Kondo M 2009 *Chem. Phys. Lett.* **478** 224
- [17] Krusing A 2004 *Opt. Lasers Eng.* **41** 329
- [18] Morita N, Ishida S, Fujimori Y and Ishikawa K 1988 *Appl. Phys. Lett.* **52** 1965
- [19] Dupont A, Caminat P and Bournot P 1995 *J. Appl. Phys.* **78** 2022
- [20] Villegas M, Caballero A C, Moure C, Duran P, Fernandez J F 1999 *J. Am. Ceram. Soc.* **82** 2411
- [21] Hutchins D A 1988 Ultrasonic generation by pulsed lasers *Physical Acoustics* vol 18 ed W P Mason and R N Thurston (New York: Academic) pp 21–123
- [22] Švrček V, Sasaki T, Katoh R, Shimizu T and Koshizaki N 2009 *Appl. Phys. B* **94** 133
- [23] Osawa E (ed) 2002 *Perspectives of Fullerenes Nanotechnology* (Dordrecht: Kluwer)
- [24] Wang Y, Yamachika R, Wachowiak A, Grobis M, Khoo K H, Lee D H, Louie S G and Crommie M F 2007 *Phys. Rev. Lett.* **99** 086402
- [25] Levchenko I, Ostrikov K, Mariotti D and Švrček V 2009 *Carbon* **47** 2379
- [26] Švrček V 2008 *Pure Appl. Chem.* **80** 2513

- [27] Tauc J, Grigorovici R and Vancu A 1966 *Phys. Status Solidi* **15** 627
- [28] Fendler J 2001 *Chem. Mater.* **13** 3196
- [29] D'Amato R, Falconieri M, Fabbri F, Bello V and Borsella E 2010 *J. Nanopart. Res.* **12** 1845
- [30] Lucovsky G, Mantini M J, Srivastava J K and Irene E A 1987 *J. Vac. Sci. Technol. B* **5** 530
- [31] Ogata Y H, Kato F, Tsuboi T and Sakka T 1998 *J. Electrochem. Soc.* **145** 2439
- [32] Guerra R and Ossicini S 2010 *Phys. Rev. B* **81** 245307
- [33] Chou J-S and Lee S-C 1995 *J. Appl. Phys.* **77** 1805
- [34] Švrček V, Fujiwara H and Kondo M 2009 *Acta Mater.* **57** 5986
- [35] Kovalev D, Heckler H, Polisski G and Koch F 1999 *Phys. Status Solidi* **251** 871
- [36] Holmes J D, Ziegler K J, Doty R C, Pell L E, Johnston K P and Korgel B A 2001 *J. Am. Chem. Soc.* **123** 3743
- [37] Yang C S, Bley R A, Kauzlarich S M, Lee H W H and Delgado G R 1999 *J. Am. Chem. Soc.* **121** 5191
- [38] Li Z F and Ruckenstein E 2004 *Nano Lett.* **4** 1463
- [39] Pradhan B, Batabyal S K and Pal A J 2006 *Appl. Phys. Lett.* **88** 93106
- [40] Oku T, Nagaoka S, Suzukia A, Kikuchi K, Hayashi Y, Inukai H, Sakuragi H and Soga T 2008 *J. Phys. Chem. Solids* **69** 1276
- [41] Chen L, Pan X, Zheng D, Gao Y, Jiang X, Xu M and Chen H 2010 *Nanotechnology* **21** 345201
- [42] Švrček V, Fujiwara H and Kondo M 2008 *Appl. Phys. Lett.* **92** 143301
- [43] Jansen H, Deboer M, Legtenberg R and Elwenspoek M 1995 *J. Micromech. Microeng.* **5** 115
- [44] Ma L L *et al* 2006 *Appl. Phys. Lett.* **88** 171907